Journal of Molecular Catalysis A: Chemical 309 (2009) 63–70

Contents lists available at ScienceDirect

Journal of Molecular Catalysis A: Chemical

journal homepage: www.elsevier.com/locate/molcata

Deactivation characteristics of Fe–Al–Cu water-gas shift catalysts in the presence of H_2S

Lingzhi Zhang[a], Jean-Marc M. Millet[b], Umit S. Ozkan[a,*]

[a] Department of Chemical and Biomolecular Engineering, The Ohio State University, 140 W. 19th Avenue, Columbus, OH 43210, USA
[b] Institut de Recherches sur la Catalyse et l'Environnement de Lyon, IRCELYON, UMR 5256 CNRS-Universiteï Claude-Bernard, Lyon 1, 2 Avenue A. Einstein, F-69626 Villeurbanne Cedex, France

ARTICLE INFO

Article history:
Received 31 January 2009
Received in revised form 20 April 2009
Accepted 23 April 2009
Available online 3 May 2009

Keywords:
Water-gas shift
Fe–Al–Cu
α-Fe_2O_3
γ-Fe_2O_3
H_2S
Deactivation mechanism
X-ray photoelectron and Mössbauer spectroscopy

ABSTRACT

This article reports the effect of H_2S exposure on the Fe-based water-gas shift catalysts and the surface and structural changes upon deactivation. Diffuse reflectance infrared Fourier transform spectroscopy was used to probe the interaction between reactants and catalyst surface before and after sulfur poisoning. X-ray photoelectron spectroscopy was used to examine the surface composition and oxidation states of the fresh and poisoned catalysts. Mössbauer spectroscopy and X-ray diffraction were used to investigate the bulk changes in the presence of H_2S. A mechanism for catalyst deactivation with H_2S was proposed by combining the reaction testing and characterization results.

1. Introduction

Hydrogen production from coal-derived synthesis gas is a promising route to provide hydrogen feedstock for chemical industry or for fuel cells. The water-gas shift (WGS) reaction is an integral step bridging a fuel gasifier and downstream H_2 purification. A variety of impurities can be found in the synthesis gas from coal gasification, among which sulfur compounds being the major ones. Under WGS conditions, sulfur is most likely to be in the form of H_2S [1]. Although in industrial operations, large desulphurization units are usually installed after the gasifier, up to a few hundred ppm levels of H_2S can still be present in coal syngas due to incomplete removal [2]. H_2S is capable of deactivating WGS catalysts. As reported by Xue et al. [1], Cu–Zn low temperature WGS catalyst is extremely sensitive to H_2S and 50 ppm H_2S can lead to complete and irreversible activity loss. Fe–Cr catalysts are more resistant to sulfur, but they still exhibit a partial decrease in activity upon sulfur exposure. Studies of catalyst deactivation in the presence of H_2S are essential to provide a fundamental understanding of interactions between H_2S and active sites and how this interaction affects the catalytic reaction between reactants and catalyst surfaces. Examination of deactivation characteristics is an indispensable step in the design of sulfur tolerant catalysts and in understanding the catalyst regeneration [3].

Because of the electronic structure of sulfur, it can bond strongly to transitional metals even at extremely low gas phase concentrations. This affinity to metal could cause marked activity loss in many catalytic reactions [4,5]. Sulfur could influence catalysts by both physical and chemical adsorption [2–4,6]. H_2S could dissociatively adsorb onto catalyst surfaces by splitting into HS^- and H^+ with the possibility of HS^- further breaking down into S^{2-}. Coordinative bonding between H_2S molecule and the surface is another type of physical adsorption [7]. These interactions could block or inhibit active sites for catalytic reaction and lead to activity loss. Chemisorption of sulfur occurs through multiple coordination sites, which could induce surface reconstruction of the metal surface. This surface rearrangement is particularly detrimental to structure-sensitive reactions. For example, the carbon formation reaction during hydrocarbon steam reforming requires a relatively large ensemble of Ni atoms [8]. Presence of a small amount of sulfur in the feedstock facilitates surface rearrangement of Ni atoms into smaller assemblies, which significantly suppresses hydrocarbon decomposition and promotes the reforming reaction [6]. Similar phenomena were observed in Pt catalytic systems where rearrangement of Pt particles caused by sulfur facilitates or suppresses certain reaction pathways [9,10].

* Corresponding author. Tel.: +1 614 292 6623; fax: +1 614 292 3769.
E-mail address: ozkan.1@osu.edu (U.S. Ozkan).

1381-1169/$ – see front matter © 2009 Elsevier B.V. All rights reserved.
doi:10.1016/j.molcata.2009.04.016

There have been extensive fundamental studies on sulfur poisoning of metals (review by Bartholomew [4]). Influence of sulfur on catalytic performance has been widely examined in different catalytic systems, such as hydrogenolysis [9], hydrogenation [5,11–13], steam reforming [6,14,15] and Fischer–Tropsch synthesis [16–21]. With increasing energy demands in recent years, coal-derived synthesis gas has been used as the feedstock for solid oxide fuel cells (SOFC). Effects of H_2S on SOFC anode materials have also been heavily investigated [2,22]. However, very few studies on H_2S effects in WGS catalytic system are available in the literature. Although sulfur-resistant WGS catalysts have been developed for conversion of raw gases from coal or crude oil gasification which contain sulfur, this molybdenum-based catalyst is only functional when a certain amount of H_2S (>1%) is present in the feed to sustain the active sites [23–25]. This limitation necessitates research on catalyst formulations that are operative both under H_2S-free and low concentration H_2S (<1000 ppm) containing feed. Progress has been reported by Xue et al. [1] and Hutchings et al. [26–30]. Xue and his coworkers evaluated a number of WGS catalysts using sulfur containing feed. Co–Cr catalysts demonstrated high WGS activity both in the absence and in the presence of H_2S (200 ppm) compared with Fe–Cr catalysts. In Hutchings and coworkers' studies, Co–MnO and $CoCr_2O_4$ catalysts exhibited high resistance to H_2S up to 240 ppm. This phenomenon was attributed to Mn and Cr functioning as sacrificial species and protecting the active Co component in the formulation. The stable spinel structure in $CoCr_2O_4$ catalysts also makes sulfidation reactions difficult. Sulfate instead of sulfide species were detected on the surface, leading only to a partial activity loss. This can be explained by the order of poisoning activity for sulfur species reported by Forzatti et al. [3]: $H_2S > SO_2 > SO_4^{2-}$. However, there are major drawbacks for Co-based WGS catalysts including lack of long term stability and methane formation due to undesired side reactions. Therefore, development of other alternative catalysts for coal-derived synthesis gas application is still needed.

In our previous work, we reported development of Cr-free WGS catalysts (Fe–Al–Cu) that were prepared by co-precipitation and sol–gel techniques [31–33]. These studies showed that Fe-only catalysts were primarily composed of α-Fe_2O_3 crystallites whereas Fe–Al–Cu comprised both α-Fe_2O_3 and γ-Fe_2O_3, with the phase composition being a strong function of the Al and Cu loadings. In freshly calcined Fe-based catalyst surface, the iron species is present in Fe_2O_3 form and converts to Fe_3O_4 after reduction. For Cu component, it starts in CuO form in calcined catalysts and is reduced to metallic Cu after reduction.

In an effort to acquire an understanding of the effect of H_2S on catalyst surface and structural properties during WGS that would assist in sulfur-tolerant catalyst design, this paper examines a series of Fe-based catalysts and the surface and structural changes that they go through as a result of H_2S poisoning. The deactivation characteristics of the catalysts were examined using different characterization techniques, including diffuse reflectance infrared Fourier transform spectroscopy (DRIFTS) to probe interaction of reactants with catalysts before and after sulfur deactivation, X-ray photoelectron spectroscopy (XPS) to examine catalyst surface composition and oxidation states upon sulfur exposure, X-ray diffraction (XRD) and Mössbauer spectroscopy to identify structural changes.

2. Experimental methods

2.1. Catalyst preparation

Fe-only, Fe–Al and Fe–Al–Cu catalysts were prepared using a sol–gel technique, which has been described in detail previously [31,32]. All chemicals were purchased from Sigma–Aldrich. Catalyst precursors were iron (III) acetylacetonate $(C_5H_8O_2)_3Fe$, aluminum nitrate $(Al(NO_3)_3{\cdot}9H_2O)$ and copper nitrate $(Cu(NO_3)_2{\cdot}3H_2O)$. C_2H_5OH and NaOH were used as the solvent and precipitating agent, respectively. The gelling temperature was maintained at 60 °C during catalyst synthesis. The pH was kept at 11 and Fe/Al molar ratio was controlled at 10. For Fe–Al–Cu catalyst, Fe/Cu ratio was kept at 5 in this work. Catalysts were calcined under air at 450 °C (ramp rate = 5 °C/min) for 4 h. The BET surface areas of all Fe catalysts that contained Al were in the range of 50 m^2/g, which was close to the surface area measured for the commercial catalyst used in this study (56 m^2/g). The Fe-only catalyst had significantly lower surface area (~20 m^2/g).

2.2. Reaction studies

All reactions were performed with a WHSV (Weight Hourly Space Velocity) = 0.06 m^3 (g cata)$^{-1}$ h^{-1} at an absolute pressure of 2 atmosphere. For catalysts evaluation in the presence of H_2S, catalysts were first reduced at 350 °C for 2 hrs in a clean simulated coal gas mixture with H_2O, CO, CO_2, H_2 and N_2 in 10/10/5/7.5/67.5 relative proportion. Fresh catalyst activity was measured with the same feed at 400 °C. To achieve steady state catalytic performance, catalysts were kept on stream for at least 10 h. After this, catalysts were treated in situ with 50 ppm H_2S/N_2 at 400 °C for a certain length of time (2.5 h in this paper). Catalytic activity was subsequently evaluated with the same clean coal gas feed as before sulfur exposure. Other details about reaction studies can be found in our previous publications [31–33].

2.3. Diffuse reflectance infrared Fourier transform spectroscopy

A Thermo 6700 FT-IR spectrometer equipped with a DRIFTS cell, an MCT detector and a KBr beam splitter was used. DRIFT spectra were collected with a 500-scan data acquisition at a resolution of 4 cm^{-1} in controlled gas atmosphere and temperature, using an environmental chamber with Zn–Se windows. For all experiments, catalysts were first pretreated in He at 450 °C for 30 min. This was followed by a reduction procedure with 10% H_2/He at 350 °C for 2 h. After reduction, the chamber was purged with He for 30 min at 400 °C and background spectra were collected after the flushing. 2% CO/He was introduced into the chamber for 15 min and a spectrum was taken. A temperature programmed reaction was performed with 2% CO and 2% H_2O (balance: He) starting from 30 °C. Temperature was ramped stepwise up to 400 °C. Spectra were collected at 30 °C, 100 °C, 200 °C, 300 °C and 400 °C after holding at each temperature for 15 min.

2.4. X-ray photoelectron spectroscopy

XPS was performed using an AXIS Ultra spectrometer, operated at 13 kV and 10 mA with monochromated Al Kα radiation (1486.6 eV). Two different sulfur treatment conditions were used: 50 ppm H_2S/N_2 at 400 °C for 24 h and 1000 ppm H_2S/N_2 at 400 °C for 72 h. At the end of the treatment, inert gas (N_2) was used to purge and cool down the reactor. The sample was sealed in N_2 before transferring to an Ar-purged glove box/transfer chamber to eliminate oxygen exposure. Charge neutralizers were used during spectra collection. All binding energies were referenced to C 1s of 284.5 eV.

2.5. Mössbauer spectroscopy

^{57}Co/Rh γ-ray source and a conventional constant acceleration spectrometer were used for spectra collection. The sulfur treatment procedure was the same as used for XPS sample preparation, but with air exposure after cooling down. All spectra were taken at

room temperature and ambient atmosphere. Isomer shifts are given with respect to α-Fe. The integrated areas under each deconvoluted signal have been used to obtain the relative populations of different iron species. An equal free-recoil fraction for all species was assumed for all iron species.

2.6. X-ray diffraction

A 9-sample holder accessory was employed to collect diffraction patterns. Sulfur-treated samples went through the same procedure used for XPS, but with air exposure after cooling down. The X-ray source was Cu Kα radiation operated at 45 kV and 20 mA. 2θ diffraction angle was varied from 20° to 90° during the measurement. International center for diffraction data (ICDD) library was used for crystal phase identification.

3. Results and discussion

3.1. Catalytic performance in the presence of H_2S

WGS catalytic performance comparison of various Fe–Al–Cu catalysts has been reported in our previous publications on the basis of equal surface area. For each catalyst in this study, fresh and poisoned catalyst activities were compared to acquire an understanding of deactivation characteristics in the presence of sulfur. Catalysts were poisoned with 50 ppm H_2S for 2.5 hrs at 400 °C and the percent activity loss for each catalyst is reported in Table 1. As shown in Table 1, both sol–gel (SG) prepared Fe–Al–Cu and commercial Fe–Cr–Cu catalysts demonstrated a partial activity loss after sulfur exposure. However, under these testing conditions, Fe-only and Fe–Al catalysts prepared by the SG method were fairly stable. It seems that presence of Cu in the catalyst accelerated the deactivation kinetics. Fe-based catalysts without Cu in the formulation showed small or no deactivation considering the error range. However, pronounced activity drop was measured for Cu-containing catalysts. A 40% decrease in CO conversion was observed for Fe–Al–Cu catalyst whereas commercial Fe–Cr–Cu lost 30% conversion after it was poisoned. The activity loss variation is consistent with Cu doping levels in these two samples. Fe–Al–Cu contains 16 wt% CuO as prepared whereas less than 5 wt% CuO is present in the commercial catalyst. To acquire an understanding of deactivation characteristics and catalyst surface and bulk changes after deactivation, extensive characterization studies were performed. To accelerate the catalyst poisoning, higher H_2S concentrations or longer exposure times were used prior to characterization.

3.2. Surface interactions between reactants and catalyst surface probed by DRIFTS

DRIFTS was employed to examine catalyst surface changes upon sulfur exposure. CO and H_2O temperature programmed reaction experiment was conducted on both freshly calcined and H_2S-poisoned (50 ppm H_2S, 400 °C for 5 h, cooled in N_2) Fe-only and Fe–Al–Cu catalysts (Fig. 1).

Fig. 1(a) illustrates species evolution with temperature for Fe-only catalysts. As seen in the figure, strong gas phase and weakly adsorbed CO bands were observed at 2180 and 2130 cm^{-1}, respectively. However, there was no CO_2 formation until a temperature of 200 °C was reached. At that point, formation of CO_2 was seen, as evidenced by bands at 2360 and 2340 cm^{-1} [33]. Over the catalyst which was poisoned by H_2S (Fig. 1(b)), similar spectra were observed, the only difference being the somewhat reduced intensity of the CO_2 bands. The picture that emerged over the Fe–Al–Cu catalyst was significantly different. Fresh catalyst showed CO_2 formation at temperatures as low as 30 °C (Fig. 1(c)). When the catalyst was poisoned, however, the decrease in the intensity of the CO_2 bands was much more pronounced (Fig. 1(d)), signaling a more severe deactivation effect with H_2S.

Table 1
WGS reaction activity percentage loss for different Fe-based catalysts upon sulfur exposure.

Catalyst	Percentage loss (%)
Fe–Al–Cu-SG	40
Fe–Cr-Cu-Commercial	30
Fe-only-SG	0
Fe–Al-SG	8

Table 2
XPS binding energies (eV) of phases present in Fe-only and Fe–Al–Cu catalysts[a].

Phases	Region	Binding energy position (eV)
Fe_2O_3	$2p_{3/2}$	710.9
Fe_3O_4	$2p_{3/2}$	710.4
FeO	$2p_{3/2}$	709.4
Fe	$2p_{3/2}$	706.6
FeS	$2p_{3/2}$	711.6
FeS_2	$2p_{3/2}$	706.8
CuO	$2p_{3/2}$	933.2
Cu	$2p_{3/2}$	932.0
Cu_2S	$2p_{3/2}$	931.5
O^{2-}	1s	529.9
S^{2-}	$2p_{3/2}$	161.2
S^{4+}	$2p_{3/2}$	166.0
SO_4^{2-}	$2p_{3/2}$	168.0

[a] Binding energies are given with a precision of 0.1 eV.

3.3. Surface changes characterized by XPS

XPS provides surface composition and oxidation state changes upon sulfur exposure. The Fe 2p, S 2p and O 1s regions of the spectra for Fe-only catalysts after experiencing different treatments are illustrated in Fig. 2. Binding energy positions for possible phases are tabulated in Table 2. As shown in the Fe 2p region (Fig. 2(a)), Fe_3O_4 was observed on reduced catalyst surface with $2p_{3/2}$ binding energy located at 710.4 eV. Two H_2S treated catalysts were examined. Fe-only-50 ppm and Fe-only-1000 ppm represent Fe-only catalysts with exposure to 50 ppm H_2S at 400 °C for 24 h and 1000 ppm H_2S at 400 °C for 72 h, respectively. This latter treatment, which involved significantly higher H_2S concentration than those found in coal gas streams that underwent desulfurization, was employed to obtain noticeable changes on catalyst surface after poisoning. As shown in Table 2, peak positions in the 2p region for Fe species are very close to each other, which create challenges for phase identification. For Fe-only-50 ppm sample, a peak centered around 710.5 eV was detected. Possible iron phases include Fe_3O_4 located at 710.4 eV ($2p_{3/2}$) due to surface reduction by H_2S and unreduced Fe_2O_3 located at 710.9 eV ($2p_{3/2}$) [34]. The peak at 706.8 eV could be attributed to FeS_2 [34]. Reactions that take place during this process could be

$$FeO_y + yH_2S \rightarrow FeS_y + yH_2O [35]$$

The actual reactions that occur are believed to be more complex as discussed later. In Twigg's review on WGS catalysis, FeS is reported as a result of Fe_3O_4 sulfidation by H_2S in reducing atmospheres [36].

$$Fe_3O_4 + H_2 + 3H_2S \rightarrow 3FeS + 4H_2O$$

Samples used in our XPS analysis were pretreated under diluted H_2S flow, with no H_2. Therefore, instead of dominant FeS, other sulfides or oxysulfides species may be formed. This can be sup-

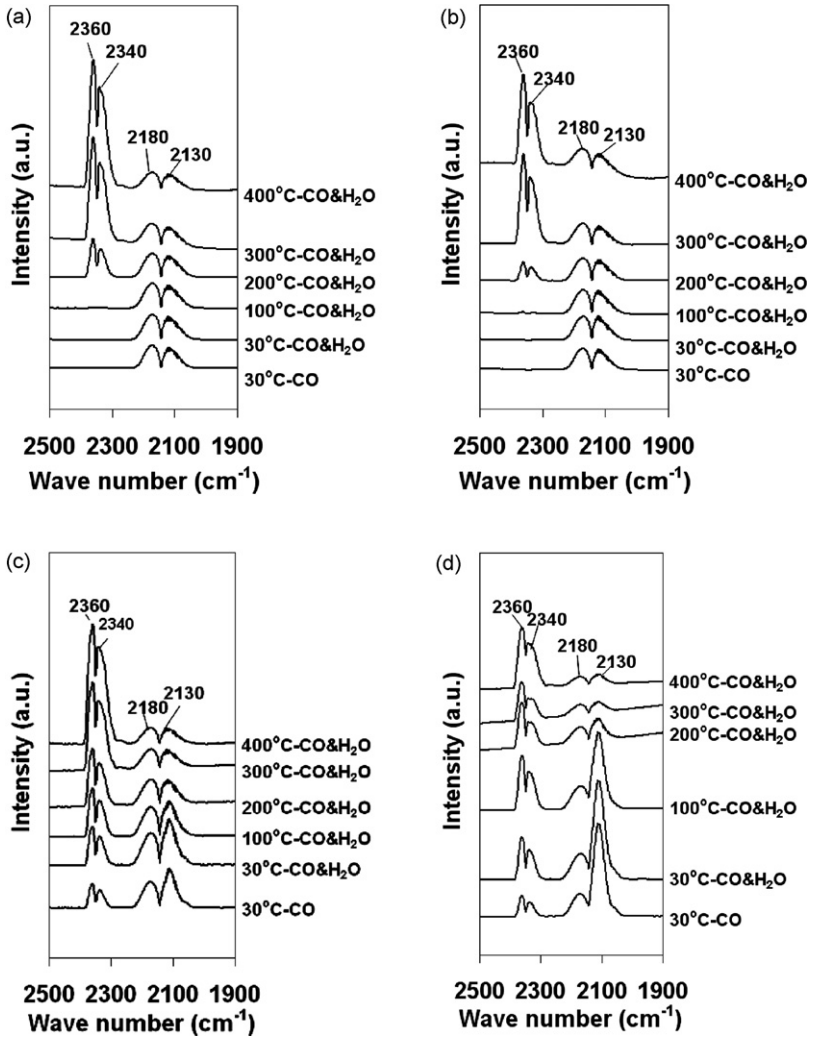

Fig. 1. DRIFT spectra during CO and H_2O temperature programmed reaction: (a) fresh Fe-only catalyst; (b) Fe-only catalyst after poisoning with 50 ppm H_2S; (c) fresh Fe–Al–Cu catalyst; (d) Fe–Al–Cu catalyst after poisoning with 50 ppm H_2S.

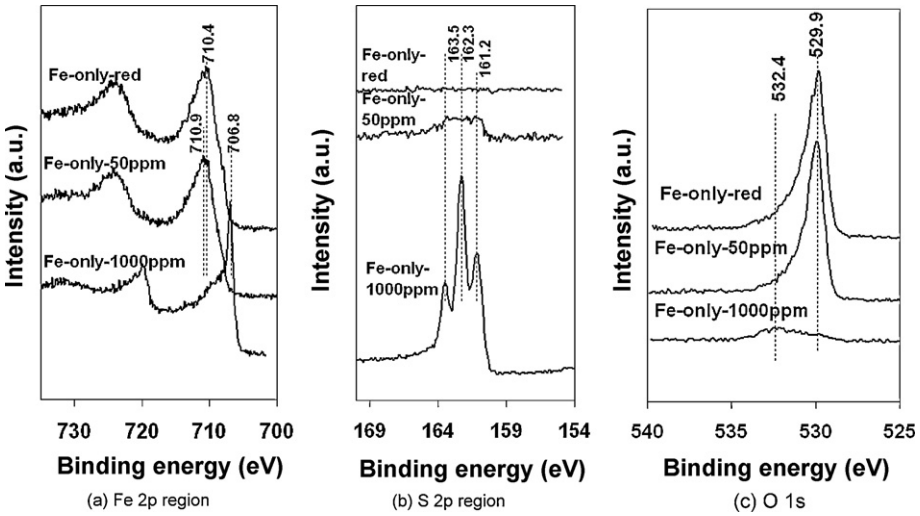

Fig. 2. X-ray photoelectron spectra for Fe-only catalysts after exposure to different concentrations of H_2S: (a) Fe 2p region; (b) S 2p region; (c) O 1s region.

ported by S 2p region analysis (Fig. 2(b)), which provides a better understanding of the sulfidation process. The peaks at 162.3 eV and 161.2 eV correspond to $2p_{1/2}$ and $2p_{3/2}$ binding energies from S^{2-}, respectively, which implies existence of FeS (Fe $2p_{3/2}$ at 711.6 eV) on poisoned samples. Different explanations can be found in the literature for the peak at 163.5 eV. In Paál et al.'s studies on sulfur poisoned Pt catalysts [10], it was suggested that elementary sulfur with a $2p_{3/2}$ binding energy located around 164 eV could be present in the sulfide entities. Bromfield and Coville [37] examined sulfided Fischer–Tropsch Fe catalysts using XPS and observed similar S 2p spectra as shown in our work. The second doublet around 163.0 eV in their work was ascribed to a different type of S^{2-} or elemental sulfur caused by decomposition of polysulfide species. A deconvolution of the S 2p spectra of the Mo-containing catalysts by Andreev et al. [23] suggested presence of subsulfides (S_{2-x}^{2-}: 160.7 eV-$2p^{3/2}$, 161.7 eV-$2p^{1/2}$), sulfides (S^{2-}: 161.8 eV-$2p^{3/2}$, 162.7 eV-$2p^{1/2}$), disulfides (S_2^{2-}: 162.6 eV-$2p^{3/2}$, 163.5 eV-$2p^{1/2}$) and elemental sulfur (S^0: 163.5 eV-$2p^{3/2}$, 164.5 eV-$2p^{1/2}$). Oxysulfide species were also reported with the S 2p region in 162.3–163.2 eV range [25], which were formed by a partial replacement of sulfur in the sulfidation product with oxygen atoms. Therefore, the S 2p region of our Fe-only poisoned catalysts could possibly consist of sulfide, subsulfide, oxysulfide and elemental sulfur species. Presence of subsulfides (FeS_2) can be further supported by Fe 2p region analysis, which showed FeS_2 band at 706.8 eV.

O 1s spectra of the same catalysts are plotted in Fig. 2(c). The O 1s spectra at 529.9 eV could be assigned to oxygen from iron oxides whereas the peak at 532.4 eV is indicative of oxygen from surface SO_x species [38], which is a result of interaction between H_2S and iron oxide species on the surface. There are marked differences in O 1s intensities from sample to sample. With 50 ppm H_2S exposure, only a small portion of the surface is sulfided (evidenced from low S 2p signals) and the Fe 2p and O 1s regions that do not display an apparent intensity decrease. With long time exposure to a much higher concentration of H_2S, sulfidation products dominate the surface. A replacement of surface oxygen by sulfur atoms takes place during sulfidation. Therefore, only a weak oxygen signal from iron oxides was detected and surface SO_x species, also with very weak signals in Fig. 2(c), were seen as a result of partial substitution of surface oxygen by sulfur.

Similar XPS spectra were collected over Fe–Al–Cu catalysts (Fe/Al = 10, Fe/Cu = 5, SG preparation). The Fe 2p regions in Fig. 3(a) exhibit the same features as the corresponding Fe-only catalysts, but with variations in intensity. More iron oxides and less FeS_2 were observed on the sample treated with 1000 ppm H_2S. Examination of the Al 2p regions for Fe–Al–Cu catalysts (results not included) did not show any noticeable intensity variations between fresh and poisoned samples, suggesting that the interaction between H_2S and Al_2O_3 is insignificant. In Ziolek et al.'s studies where H_2S adsorption on metal oxides [7] was examined, a small amount of sulfur adsorption (~0.2 wt% sulfur) was detected on Al_2O_3. This discrepancy could possibly be caused by H_2S adsorption conditions employed in their work, in which ~2.8 volume% H_2S was adsorbed onto bulk Al_2O_3. The Cu 2p region (Fig. 3(b)) for sulfided samples is speculated to be a mixture of metallic Cu (932.0 eV-$2p_{3/2}$) and Cu_2S (931.5 eV-$2p_{3/2}$) [34]. X-ray photoelectron spectra of the Cu 2p region cannot provide the resolution required for clear differentiation. However, presence of Cu_2S was confirmed by characterization results presented in the following sections. For the S 2p region (Fig. 3(c)), in addition to possible sulfide, subsulfide and oxysulfide species in poisoned Fe-only catalysts, a low intensity peak around 168 eV appeared, which is caused by sulfate species. Sulfate species may be formed as a result of sulfide species oxidation. This could occur either during the H_2S treatment step using neighboring surface oxygen or due to a surface phase rearrangement between sulfur and oxygen atoms under H_2S lean conditions [22]. O 1s region also implies formation of SOx as discussed earlier.

The reduction–oxidation cycle has been discussed in our previous publication on Fe-based catalysts [33]. The active phase for WGS is Fe_3O_4 (magnetite), which has an inverse spinel structure that can be represented as $(Fe_8^{3+})_A(Fe_8^{3+}Fe_8^{2+})_BO_{32}$. "A" and "B" represent tetrahedral and octahedral sites, respectively. During the reaction, the electron transfer between Fe^{2+} and Fe^{3+} in the octahedral sites in Fe_3O_4 promotes CO oxidation and H_2O reduction reactions to produce CO_2 and H_2. Cu can play a dual role, by providing active sites (possibly with higher intrinsic activity) and by improving electron transfer properties between Fe^{2+} and Fe^{3+} during WGS. As can be seen from declining surface oxygen coverage and rising surface sulfur coverage, when catalysts are exposed to H_2S, sulfur could replace oxygen in iron oxide structure. Although change in surface Fe signal intensity is not very pronounced, formation of FeS_x species diminishes WGS performance. More importantly, sulfur could interact strongly with Cu promoter and form Cu_2S. Once Cu on the surface is poisoned, it possibly acts as an inert diluent and does not function as a promoter any more, which explains the marked activity loss for Cu-containing catalysts (Table 1). Lahtinen et al. studied influence of sulfur poisoning on CO adsorption on Co (0 0 0 1) surface. It was revealed from their work that adsorption of CO on sulfur-exposed surface decreases significantly. More importantly, a redistribution of CO adsorption sites on the surface

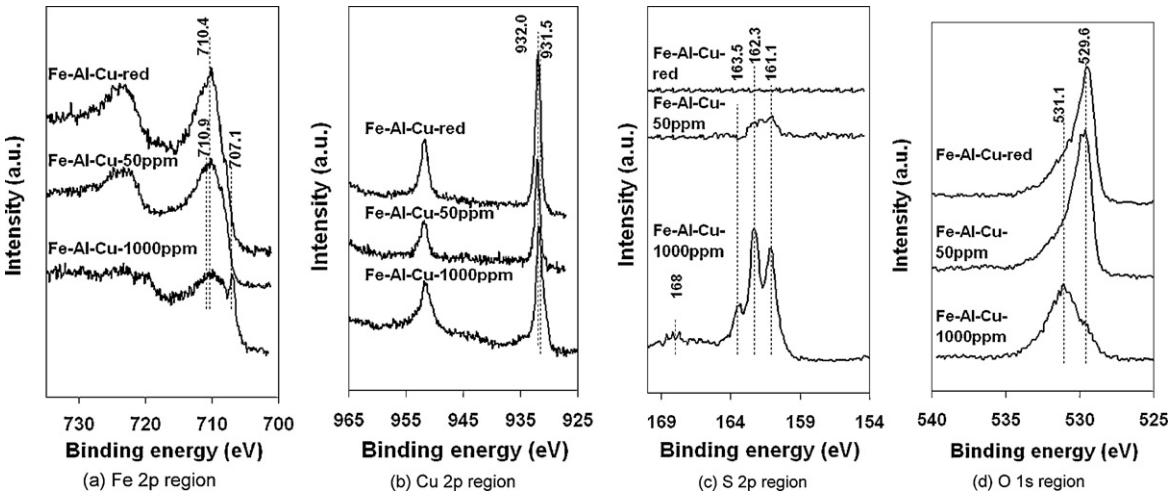

Fig. 3. X-ray photoelectron spectra for Fe–Al–Cu catalysts after exposure to different concentrations of H_2S: (a) Fe 2p region; (b) Cu 2p region; (c) S 2p region; (d) O 1s region.

is induced by the presence of sulfur [39]. It is possible that surface changes upon exposure to sulfur may decrease the available CO adsorption sites in our work as well. Additionally, hindrance of electron transfer in the redox cycle greatly decelerates the progression of the WGS reaction.

3.4. Phase composition and oxidation states examined by Mössbauer spectroscopy

Mössbauer spectroscopy was used to examine catalyst composition and iron oxidation states in the bulk phases. 1000 ppm H_2S/N_2 was used to poison Fe–Al–Cu (Fe/Al = 10, Fe/Cu = 5, SG preparation) catalysts at 400 °C for 72 h. This is the same procedure used prior to XPS analysis. However, unlike the XPS analysis, samples were exposed to air after H_2S treatment and spectra were collected under ambient atmosphere. Spectrum for the freshly calcined Fe–Al–Cu has been discussed previously [31,32] and is included here for comparison (Fig. 4(a)). Fresh Fe–Al–Cu consists primarily of small promoter substituted γ-Fe_2O_3 particles, with a small portion of large γ-Fe_2O_3 particles (>20 nm). All spectra were deconvoluted to fit different iron species. Hyperfine parameters obtained from the fits (for both freshly calcined and H_2S-poisoned Fe–Al–Cu catalysts) are listed in Table 3. Integrated area for each species is used to obtain its relative abundance. The spectrum of the poisoned Fe–Al–Cu catalyst shown in Fig. 4(b) has been fitted with one doublet and five sextets. The doublet has been attributed (as reported previously for calcined Fe–Al–Cu) to superparamagnetic substituted γ-Fe_2O_3 or partially to α-Fe_2O_3 small particles. The presence of a valleriite type phase, which is a hydroxysulfide of Fe and Cu cannot be totally excluded since it is characterized by a signal with $\delta = 0.45$ and $\Delta = 0.55$ [40]. This signal, which is the major one and accounts for 60% of the iron atoms, should correspond to unreacted iron oxide species (promoter) as observed in calcined catalysts. This also suggests that a majority of the iron oxide particles remain intact even after exposure to high concentrations of H_2S (1000 ppm). The three sextets characterized by internal magnetic field, respectively, corresponding to 30.4, 26.1 and 23.1 T and presenting approximately equal relative intensities are assigned to $Fe_{1-x}S$ with pyrrhotite type structure [41]. The sextet with the largest internal magnetic field and the negative quadrupolar splitting can also unambiguously be attributed to large particles (>20 nm) of α-Fe_2O_3 [42]. Presence of α-Fe_2O_3 is not surprising as evidenced from XRD analysis in the following section. The last sextet with an internal magnetic field equal to 35.3 T has been attributed to the phase $CuFeS_2$ with chalcopyrite type structure [40].

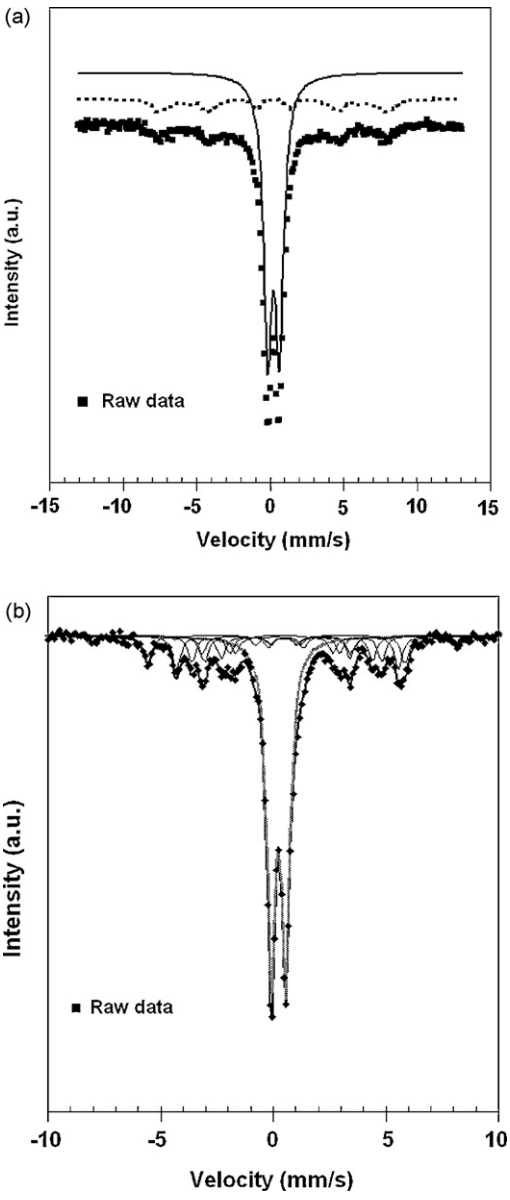

Fig. 4. Mössbauer spectra of: (a) freshly calcined Fe–Al–Cu catalysts; (b) Fe–Al–Cu catalysts poisoned with 1000 ppm H_2S/N_2 at 400 °C for 72 h.

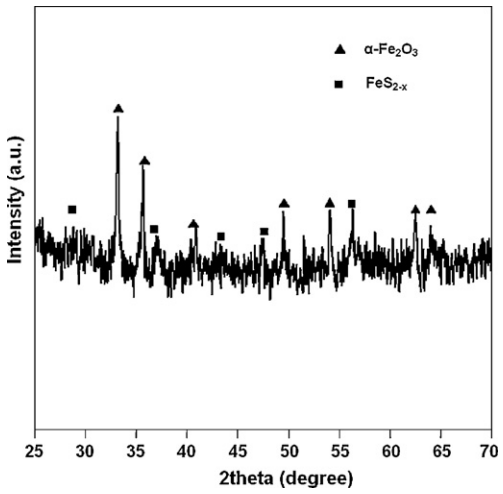

Fig. 5. X-ray diffraction pattern of commercial FeS after air exposure.

FeS is extremely air sensitive and decomposes readily to FeS_x and α-Fe_2O_3 even at room temperature, as seen in XRD analysis on commercial FeS reference (Fig. 5), which also explains why no stoichiometric FeS was detected in the poisoned sample. $Fe_{1-x}S$ is probably formed as a result of coordination environment changes among Fe, S and O atoms [41].

3.5. Crystal phases examined by XRD analysis

XRD was used to provide information on crystal phases present for calcined and poisoned catalysts. Freshly calcined and H_2S-poisoned catalysts (50 ppm H_2S (400 °C, 24 h) and 1000 ppm (400 °C, 72 h)), which are the same as the samples for XPS and Mössbauer analysis, were examined. XRD patterns are shown in Fig. 6(a) for Fe-only catalysts and Fig. 6(b) for Fe–Al–Cu catalysts.

The dominant crystal phase for calcined Fe-only catalyst is α-Fe_2O_3. For the Fe-only-50 ppm catalyst, Fe_3O_4 phase was observed, which results from α-Fe_2O_3 reduction. No sulfur-related phases were detected. As reported in the literature [43], when H_2S concen-

Table 3
Mössbauer parameters derived from the sample spectra collected at 25 °C[a].

Sample	Splitting	Relative intensity (%)	δ (mm/s)	Δ, ε (mm/s)	H (T)
Fe–Al–Cu-SG (Fe/Al = 10, Fe/Cu = 5)	Doublet	84	0.34	0.80	0
	Sextet	16	0.34	0.00	47.2
Fe–Al–Cu-SG-H_2S (Fe/Al = 10, Fe/Cu = 5)	Doublet	60	0.33	0.65	0
	Sextet	11	0.69	0.07	30.4
	Sextet	9	0.66	0.08	26.1
	Sextet	9	0.68	0.18	23.1
	Sextet	9	0.23	0	35.3
	Sextet	2	0.32	−0.20	50.0

[a] δ: isomer shift (referred to α-Fe), Δ and ε: quadrupolar splitting in a quadrupolar doublet and in a magnetic sextet, respectively, H: internal magnetic field.

tration is low, only surface sulfide species will be formed because bulk sulfide is not thermally stable. However, Fe-only catalyst poisoned by 1000 ppm H_2S demonstrates the presence of both FeS_{2-x} and α-Fe_2O_3, which are likely products from iron sulfide species decomposition in air, as shown in the XRD pattern in Fig. 6. It is also noted that the diffraction lines for this catalyst are narrow and intense, implying that large crystals are generated during the sulfidation and oxidation process. Calcined Fe–Al–Cu catalysts are composed of γ-Fe_2O_3 phase whereas Fe–Al–Cu-50 ppm consists of Fe_3O_4 crystallites. After exposure to 1000 ppm H_2S, Fe–Al–Cu catalysts contain multiple crystal phases: γ-Fe_2O_3, α-Fe_2O_3, FeS_{2-x} and Cu_2S. This provides complementary information to Mössbauer results and confirms some of the assignments as well. Both iron and copper sulfided crystallites were detected. Another observation from XRD patterns presented in Fig. 6 is that larger α-Fe_2O_3 crystals were formed on poisoned Fe-only catalyst compared to poisoned Fe–Al–Cu catalyst. This result was clearly confirmed by Mössbauer spectroscopy showing only 2% of iron species to be of larger α-Fe_2O_3 particles in Fe–Al–Cu catalysts after H_2S treatment (Table 3). This could be explained by the presence of promoters that can prevent or minimize aggregation of iron species to form large crystallites.

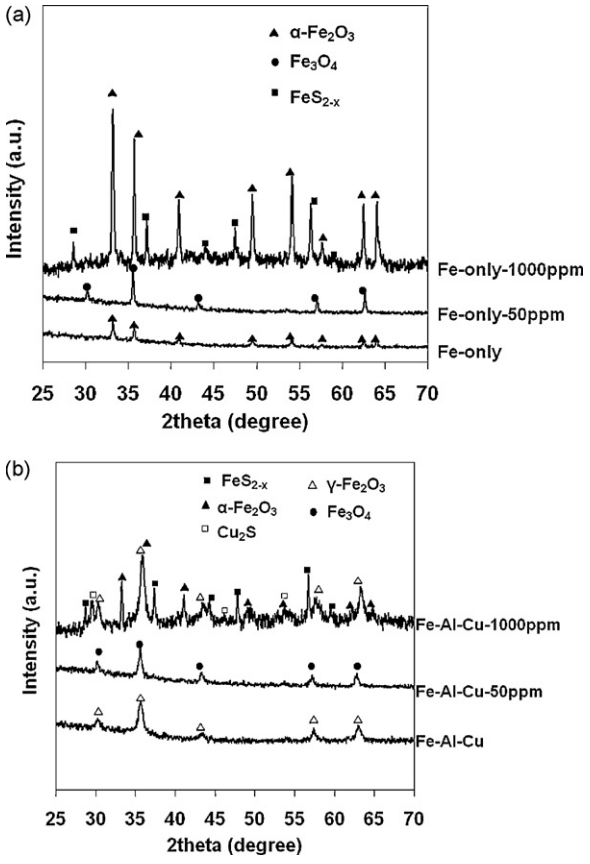

Fig. 6. X-ray diffraction patterns of freshly calcined and sulfur poisoned catalysts: (a) Fe-only catalyst; (b) Fe–Al–Cu catalysts.

4. Summary

A series of Fe-based catalysts were evaluated for WGS reaction and characterized after they were exposed to H_2S. Catalysts exhibited activity loss to different extents. Cu-containing catalysts were more sensitive to H_2S and showed faster deactivation kinetics compared to Cu-free samples. Characterization results suggest that, upon sulfur exposure, catalyst surface oxygen is partially replaced by sulfur, leading to pronounced changes in Fe and Cu coordination environment. Catalyst activity loss can be attributed to changes in the surface active sites induced by FeS, $CuFeS_2$ and CuS_2 formation, impeding the redox electron transfer cycle during WGS, with Cu being more susceptible to H_2S poisoning and contributing more severely to initial activity loss.

Acknowledgments

The financial contributions from the Ohio Coal Development Office and the Ohio Department of Development through the Wright Center of Innovation Program are gratefully appreciated.

References

[1] E. Xue, M. O'Keeffe, J.R.H. Ross, Catal. Today 30 (1996) 107.
[2] M. Gong, X. Liu, J. Trembly, C. Johnson, J. Power Sources 168 (2007) 289.
[3] P. Forzatti, L. Lietti, Catal. Today 52 (1999) 165.
[4] C.H. Bartholomew, P.K. Agrawal, J.R. Katzer, Adv. Catal. 31 (1982) 135.
[5] J. Barbier, E. Lamy-pitara, P. Marecot, J.P. Boitiaux, J. Cosyns, F. Verna, Adv. Catal. 37 (1990) 279.
[6] M.S. Kim, N.M. Rodriguez, R.T.K. Baker, J. Catal. 143 (1993) 449.
[7] M. Ziolek, J. Kujawa, O. Saur, J.C. Lavalley, J. Mol. Catal. A: Chem. 97 (1995) 49.
[8] J.H. Edwards, A.M. Maitra, Fuel Process. Technol. 42 (1995) 269.
[9] C. Kim, G.A. Somorjai, J. Catal. 134 (1992) 179.
[10] Z. Paál, K. Matusek, M. Muhler, Appl. Catal. A: Gen. 149 (1997) 113.
[11] M.V. Twigg, M.S. Spencer, Appl. Catal. A: Gen. 212 (2001) 161.
[12] L. Hu, G. Xia, L. Qu, M. Li, C. Li, Q. Xin, D. Li, J. Catal. 202 (2001) 220.
[13] N.S. Fígoli, P.C. L'Argentiere, A. Arcoya, X.L. Seoane, J. Catal. 155 (1995) 95.
[14] P.K. Cheekatamarla, A.M. Lane, J. Power Sources 153 (2006) 157.
[15] J.J. Strohm, J. Zheng, C. Song, J. Catal. 238 (2006) 309.
[16] C.H. Bartholomew, R.M. Bowman, Appl. Catal. 15 (1985) 59.
[17] N. Koizumi, K. Murai, T. Ozaki, M. Yamada, Catal. Today 89 (2004) 465.
[18] J. Li, N.J. Coville, Appl. Catal. A: Gen. 208 (2001) 177.
[19] M. Yamada, N. Koizumi, T. Miyazawa, T. Furukawa, Catal. Lett. 78 (2002) 195.
[20] Z.-T. Liu, J.-L. Zhou, B.-J. Zhang, J. Mol. Catal. 94 (1994) 255.
[21] A.L. Chaffee, I. Campbell, N. Valentine, Appl. Catal. 47 (1989) 253.
[22] J.N. Kuhn, N. Lakshminarayanan, U.S. Ozkan, J. Mol. Catal. A: Chem. 282 (2008) 9.
[23] A.A. Andreev, V.J. Kafedjiysky, R.M. Edreva-Kardjieva, Appl. Catal. A: Gen. 179 (1999) 223.
[24] R.N. Nickolov, R.M. Edreva-Kardjieva, V.J. Kafedjiysky, D.A. Nikolova, N.B. Stankova, D.R. Mehandjiev, Appl. Catal. A: Gen. 190 (2000) 191.
[25] D. Nikolova, R. Edreva-Kardjieva, G. Gouliev, T. Grozeva, P. Tzvetkov, Appl. Catal. A: Gen. 297 (2006) 135.
[26] F.M. Gottschalk, R.G. Copperthwaite, M. Van Der Riet, G.J. Hutchings, Appl. Catal. 38 (1988) 103.
[27] F.M. Gottschalk, G.J. Hutchings, J. Chem. Soc., Chem. Commun. (1988) 123.

[28] R.G. Copperthwaite, F.M. Gottschalk, T. Sangiorgio, Appl. Catal. 63 (1990) L11.
[29] G.J. Hutchings, R.G. Copperthwaite, F.M. Gottschalk, R. Hunter, J.R. Mellor, S.w. Orchard, T. Sangiorgio, J. Catal. 137 (1992) 408.
[30] F.M. Gottschalk, G.J. Hutchings, Appl. Catal. 51 (1989) 127.
[31] L. Zhang, X. Wang, J.-M.M. Millet, P.H. Matter, U.S. Ozkan, Appl. Catal. A: Gen. 351 (2008) 1.
[32] L. Zhang, J.-M.M. Millet, U.S. Ozkan, Appl. Catal. A: Gen. 357 (2008) 66.
[33] S. Natesakhawat, X. Wang, L. Zhang, U.S. Ozkan, J. Mol. Catal. A: Chem. 260 (2006) 82.
[34] J.F. Moulder,W.F. Stickle, P.E. Sobol, K.D. Bomben, J. Chastain, Handbook of X-ray Photoelectron Spectroscopy, Perkin-Elmer Corporation, 1992.
[35] S.S. Tamhankar, M. Bagajewlcz, G.R. Gavalas, Ind. Eng. Chem. Process. Des. Dev. 25 (1986) 429.
[36] M.V. Twigg, Catalyst Handbook, 2nd. Ed., ICI, Wolf Publishing Ltd, London, 1989.
[37] T.C. Bromfield, N.J. Coville, Appl. Surf. Sci. 119 (1997) 19.
[38] R.M. Ferrizz, R.J. Gorte, J.M. Vohs, Catal. Lett. 82 (2002) 123.
[39] K. Habermehl-Ćwirzeń, J. Lahtinen, Surf. Sci. 573 (2004) 183.
[40] N.I. Chistyakova, T.V. Gubaidulina, V.S. Rusakov, J. Phys. 56 (2006) E123.
[41] N.N. Greenwood, T.C. Gibb, Mössbauer Spectroscopy, Chapman and Hall Ltd, London, 1971.
[42] G. Doppler, A.X. Trautwein, H.M. Ziethen, Appl. Catal. 40 (1988) 119.
[43] Z. Cheng, M. Liu, Solid State Ionics 178 (2007) 925.